JOURNAL OF GEOPHYSICAL RESEARCH, VOL. 108, NO. C3, 8055, doi:10.1029/2001JC001004, 2003

A semiempirical model of the normalized radar cross section of the sea surface, 2. Radar modulation transfer function

Vladimir Kudryavtsev

Marine Hydrophysical Institute, National Academy of Science, Sebastopol, Ukraine

Nansen International Environmental and Remote Sensing Center, St. Petersburg, Russia

Danièle Hauser and Gérard Caudal

Centre d'Etude des Environnements Terrestres et Planétaires, Centre National de la Recherche Scientifique (CNRS), Universitéde Versailles, Velizy, France

Bertrand Chapron

Laboratoire d' Océanographie Spatiale, Institut Francais de Recherche pour l'Exploitation de la Mer, Plouzané, France

Received 23 May 2001; revised 2 May 2002; accepted 20 May 2002; published 10 January 2003.

[1] Multiscale composite models based on the Bragg theory are widely used to study the normalized radar cross section (NRCS) over the sea surface. However, these models are not able to correctly reproduce the NRCS in all configurations. In particular, even if they may provide consistent results for vertical transmit and receive (VV) polarization, they fail in horizontal transmit and receive (HH) polarization. In addition, there are still important discrepancies between model and observations of the radar modulation transfer function (MTF), which relates the modulations of the NRCS to the long waves. In this context, we have developed a physical model that takes into account not only the Bragg mechanism but also the non-Bragg scattering associated with radio wave scattering from breaking waves. The same model was built to explain both the background NRCS and its modulation by long surface wave (wave radar MTF problem). In part 1, the background NRCS model was presented and assessed through comparisons with observations. In this part 2, we extend the model to include a third underlying scale associated with longer waves (wavelength $\sim$10–300 m) to explain the modulation of the NRCS. Two contributions are distinguished in the model, corresponding to the so-called tilt and hydrodynamic MTF. Results are compared to observations (already published in the literature or derived from the FETCH experiment). As found, taking into account modulation of wave breaking (responsible for the non-Bragg mechanism) helps to bring the model predictions in closer agreement with observations. In particular, the large MTF amplitudes for HH polarization (much larger than for VV polarization) and MTF phases are better interpreted using the present model. *INDEX TERMS:* 4275 Oceanography: General: Remote sensing and electromagnetic processes (0689); 4560 Oceanography: Physical: Surface waves and tides (1255); 4504 Oceanography: Physical: Air/sea interactions (0312); 4506 Oceanography: Physical: Capillary waves; *KEYWORDS:* radar cross-section, ocean surface, surface gravity waves, wave breaking, modulation transfer function, non-Bragg scattering

Citation: Kudryavtsev, V., D. Hauser, G. Caudal, and B. Chapron, A semiempirical model of the normalized radar cross section of the sea surface, 2, Radar modulation transfer function, *J. Geophys. Res.*, *108*(C3), 8055, doi:10.1029/2001JC001004, 2003.

1. Introduction

[2] Multiscale models based on the Bragg theory are generally found to fail reproducing satisfactorily the behavior of the normalized radar cross section (NRCS) over a large range of radar frequencies, incidence angles, environmental conditions (wind and waves) and for the different polarization states. In particular models, which may provide consistent results for vertical transmit and receive (VV) polarization, are not in agreement with observations for horizontal transmit and receive (HH) polarization [e.g., *Plant*, 1990; *Janssen et al.*, 1998]. In addition, models based on the same theory to predict the modulations of radar cross section along the longer waves, also exhibit discrepancies with reported measurements. This is particularly true for the HH polarization [*Schmidt et al.*, 1995].

0148-0227/03/2001JC001004$09.00

[3] In this context, the general goal of this set of two papers (parts 1 and 2) is to present a semiempirical model of the NRCS which is consistent, in terms of both mean and modulation, with VV and HH polarized radar observations over a large range of radio wave frequencies and incidence angles. In part 1, we presented the model describing the statistical properties of the sea surface (including statistical characteristics of wave breaking events), and the related radar backscattering model including Bragg and non-Bragg scattering. In this part 2, we extend these developments to infer the wave radar modulation transfer function (MTF).

[4] As defined, the MTF is the linear response function relating the slope of the long waves to the wave-induced variation of the radar return [*Keller and Wright*, 1975]. Two contributions are usually distinguished, tilt and hydrodynamic, respectively. The tilt modulation of NRCS results from changes of the local incidence angle along the long wave (LW) profile. The hydrodynamic part of the radar MTF describes the contribution to the total MTF of the modulation associated with the scattering characteristics along the LW profile. Field experiments have been deployed in the past to estimate the radar MTF [e.g., *Plant et al.*, 1983; *Schroeder et al.*, 1986; *Schmidt et al.*, 1995; *Keller and Plant*, 1990; *Grodsky et al.*, 1999]. The collected measurements give a consistent picture of the MTF dependence with respect to the radar frequency, the wind speed, and the LW characteristics. The main features experimentally established are a well-pronounced dependence of the MTF with wind speed (except maybe in L-band) with a decreasing MTF amplitude with increasing wind speeds, an increase of the MTF amplitude with decreasing LW frequency, and an amplification of the radar scattering in the vicinity of wave crests. Under a pure Bragg scattering model, the magnitude of the tilt contribution is wind independent, and its phase follow the LW slope. Consequently, all of these measured features must certainly be attributed to the hydrodynamic MTF. Moreover, another important experimental result related to the hydrodynamic MTF, is that its magnitude found for HH polarization (after subtracting the tilt component) is larger than that found from the VV polarization [e.g., *Hara and Plant*, 1994; *Schmidt et al.*, 1995]. Following the Bragg theory and using the wave action conservation equation written in the relaxation approximation [*Alpers and Hasselmann*, 1978], some success has been obtained to relate the measurements and the straining effects associated with the LW orbital velocity field. However, such effects should be strongly attenuated as the radar frequency increases. This has not been generally observed. To explain the observed MTF features, *Hara and Plant* [1994], *Romeiser et al.* [1994], and others suggested a wind stress modulation mechanism. This mechanism assumes a modulation of the Bragg waves associated with strong variations of wind surface stress along the LW profiles. According to the observations, this assumption implies that the magnitude of this modulation is very large (normalized amplitude 10 times larger than the LW steepness) and with a marked intensification near the LW crests. However, in all these studies, it was mentioned that there is no experimental evidence showing such strong wind stress variation in reality.

[5] In the present development, we wish to emphasize the expected potential impact associated with the nonhomogeneous distribution along the LWs of small-scale breaking waves. As developed in part 1, our NRCS model takes into account both the Bragg and non-Bragg scattering mechanisms. The latter is associated with microwave scattering from breaking waves. Model calculations and comparison with available measurements presented in part 1, showed that radio wave scattering from breaking waves could significantly contribute to the NRCS at moderate incidence angles, especially for HH polarization. Field observations by *Dulov et al.* [2002] show that the breaking waves are very strongly modulated by the dominant surface waves: the normalized modulation amplitude was found about 20 times larger than the LW slope. While the wave breaking contribution to the background NRCS might be small, one can expect that large modulations of breaking waves significantly affect the radar MTF.

[6] To analyze the hydrodynamic MTF we will thus consider three contributions. The first one results from the modulations of the short wave (SW) spectrum at the Bragg wave number. Following our two-scale development, the second contribution is associated with the mean square slope modulations of the second scale (tilting waves) by the third LW scale. Finally, the third contribution comes from the modulations of the wave breaking parameters by LW. *Romeiser et al.* [1994] developed their MTF model accounting for the first two contributions (Bragg waves and slope of the second scale). The impact of the modulation of wave breaking on the radar MTF has never been analyzed. We will show that this mechanism may play a crucial role in the radar MTF at both HH and VV polarizations. In addition, this mechanism could explain the observed difference between VV and HH measurements, predicting larger amplitudes of the hydrodynamic MTF for HH polarization. To our knowledge, these features have never been consistently reproduced within the frame of a Bragg scattering model (neither pure Bragg model nor three-scale composite model).

[7] It must be emphasized that, in our analysis, the description of SW and wave breaking modulations, and their subsequent contributions to the radar MTF, are based on the same energy balance equation. Furthermore, the model is based on a self-consistent description of the background NRCS of the sea surface and its modulations by dominant surface waves.

[8] In section 2, we present the main equations for the tilt and hydrodynamic parts of the radar MTF. In each case, the contributions of Bragg and non-Bragg scattering processes are described. Section 3 presents the model describing the modulations of the SW spectrum. Results for the different components of the radar MTF model are presented in section 4, while section 5 is devoted to the comparison between model results and observations (data already published and data processed for this study from the FETCH experiment). Conclusions are presented in section 6.

2. Radar MTF

[9] The radar MTF describes the linear response of the sea surface radar backscatter in the presence of long surface waves (LW). The term LW implies that the wavelength of these longer waves is much larger than the correlation length associated with the shorter waves. Let us assume

that a LW with amplitude A and wave number K is running along the x_1 axis:

$$\zeta(x,t) = \frac{1}{2}\left(Ae^{i(Kx-1-\Omega t)} + c.c\right) \quad (1)$$

where c.c refers to the complex conjugate. Under a linear modulation model, this LW will induce a small variation of the sea surface NRCS, so that $\sigma_0^p = \bar{\sigma}_0^p + \tilde{\sigma}_0^p$ where the upper index p stands for HH or VV polarization, $\bar{\sigma}_0^p$ is the mean NRCS and $\tilde{\sigma}_0^p$ is the variation in the presence of the LW:

$$\tilde{\sigma}_0^p(x,t) = \frac{1}{2}\left(\hat{\sigma}_0^p Ae^{i(Kx-1-\Omega t)} + c.c\right) \quad (2)$$

where $\hat{\sigma}_0^p$ is a complex amplitude. The radar MTF M was originally introduced by *Keller and Wright* [1975] and in our notations it reads:

$$M_\sigma^p = \frac{\hat{\sigma}_0^p}{\bar{\sigma}_0^p(KA)} \quad (3)$$

Note that throughout the paper we use the term MTF to describe the LW-induced modulation of any quantity Y. So that the definition of the MTF M_Y is:

$$M_Y = \frac{\hat{Y}}{(KA\overline{Y})} \quad (4)$$

where $\hat{Y}$ is the complex amplitude of the harmonic response of quantity Y to the LW (1), and $\overline{Y}$ is its mean value. Negative imaginary part of $\hat{Y}$ means that maximum of Y variation is shifted on the forward slope of the LW and vice versa. Correspondingly, in all figures below, positive MTF phase means that maximum of a Y variation is located on the forward LW slope.

2.1. Governing Equations

[10] To study the radar MTF problem we use the semi-empirical model presented in part 1. In the frame of this model, we consider moderate incident angles θ ($20° < \theta < 70°$), and the NRCS σ_0^p is presented as a sum of a two-scale Bragg scattering part σ_{br}^p, and a non-Bragg scattering part σ_{wb}:

$$\sigma_0^p = \sigma_{br}^p + \sigma_{wb} \quad (5)$$

For the radar MTF problem, the NRCS for the Bragg part is written as:

$$\sigma_{br}^p(\theta,\varphi) = \sigma_{0br}^p(\theta,\varphi)\left(1 + g^p\overline{\nabla\zeta^2}\right) \quad (6)$$

where φ is the radar look direction, $\sigma 0_{br}^p$ is the NRCS for the pure Bragg scattering defined by the surface elevation spectrum $F_r(k_{br},\varphi)$ at the Bragg wave number k_{br}

$$\sigma_{0br}^p = 16\pi k_r^4 |G_p(\theta)|^2 F(k_{br},\varphi) \quad (7)$$

$k_{br} = 2k_r \sin\theta$, k_r is the radar wave number, θ is incidence angle, $G_p(\theta)$ is the Bragg scattering geometric coefficient, g_p is the coefficient accounting for the tilting effect of longer surface waves carrying Bragg waves (see part 1 for more details). With respect to the expression of g_p used in part 1 (see part 1, equation (33)), a simplified form is used here by omitting the cross-polarization term, so that

$$g^p = \left(4\sigma_{0br}^p\right)^{-1}\partial^2\sigma_{0br}^p/\partial\theta^2 \quad (8)$$

In (6), $\overline{\nabla\zeta^2}$ is the mean square slope (mss) of the so-called tilting waves associated with the second scale. It is given by:

$$\overline{\nabla\zeta^2} = \int\int_{k<k-t} B(k,\varphi')d\varphi' d\ln k \quad (9)$$

where k_t is the upper limit of the tilting waves range (chosen as $k_t = 1/5k_{br}$), B is the curvature spectrum (defined as $B(k) = k^4F(k)$).

[11] The NRCS associated with the non-Bragg scattering is written as:

$$\sigma_{wb}(\theta) = \sigma_{0wb}(\theta)q \quad (10)$$

where $\sigma_{0wb}(\theta)$ is the NRCS of the surface areas with enhanced roughness generated by breaking waves and was defined in part 1 as

$$\sigma_{0wb}(\theta) = \left(\sec^4\theta/s_{wb}^2\right)\exp\left(-\tan^2\theta/s_{wb}^2\right) + \varepsilon_{wb}/s_{wb}^2 \quad (11)$$

s_{wb}^2 is the mean square slope of the breaker surface (assumed isotropic and wind independent), ε_{wb} is a constant proportional to the ratio of breaker thickness to its length, and q is the fraction of the sea surface covered by breaking zones. Quantity q is parameterized via the length of the breaking fronts $\Lambda(\mathbf{k})$ of the wind waves with wave number vectors $\mathbf{k}$ in the range from $\mathbf{k}$ to $\mathbf{k} + d\mathbf{k}$ as:

$$q = C_q\int_{k<k-nb} k^{-1}\Lambda(\mathbf{k})d\mathbf{k} \quad (12)$$

It is important to recall that in the equilibrium gravity range of the spectrum, $\Lambda(\mathbf{k})$ is a function of the saturation spectrum $B(\mathbf{k})$ parameterized according to equation (57) in part 1. As explained in part 1, C_q is a constant of the order of 10, $k_{nb} = 0.1k_r$ (k_r is radar wave number) is the upper limit of the range of breaking waves providing non-Bragg scattering, and constants s_{wb}^2 and ε_{wb} in (11) are $s_{wb}^2 = 0.19$, $\varepsilon_{wb} = 0.05$. In the equilibrium gravity range of the spectrum, $\Lambda(\mathbf{k})$ is a function of the saturation spectrum (part 1, equation (57)).

[12] For the NRCS of the Bragg part (6), we neglect here the cross correlation between tilt and hydrodynamic modulations. As discussed in part 1, this term does not significantly contribute to the NRCS. In the pure tilt effect, we further neglect here the angular dependence of the mean square slope of tilting waves. In the non-Bragg scattering component, we also omit the term responsible for the anisotropy in azimuth. Throughout the paper we will need estimates of the contribution of wave breaking (non-Bragg scattering) to the total NRCS: $P^p(\theta) = \sigma_{wb}(\theta)/\sigma_0^p(\theta)$.

[13] This quantity is shown in Figure 1 as a function of incidence angle for C-band (radar wavelength about 5 cm), VV and HH polarization, and for wind speeds of 5 and 15 m

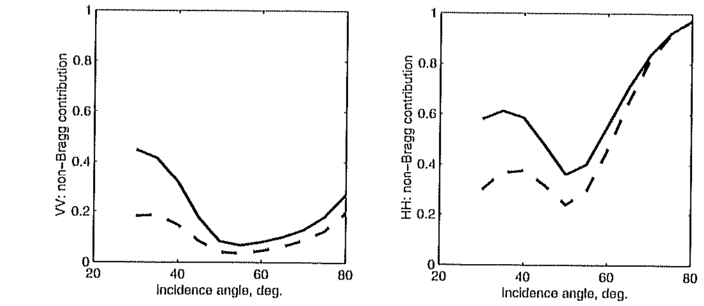

Figure 1. Ratio of non-Bragg scattering to the total NRCS ($P^p = \sigma_{wb}/\sigma_0^p$) as a function of the incidence angle for a wind speed of 5 m/s (dashed lines) and 15 m/s (solid lines). C-band, VV polarization (left plot), HH polarization (right plot).

s^{-1}. At VV polarization, the contribution of the non-Bragg scattering is small, less than 20% (except for small incidence angles and high wind conditions, where P^{vv} reaches 40%). At HH polarization the impact of wave breaking on the NRCS is stronger, but remains less than 50% in the intermediate range of incidence angles ($40° \leq \theta \leq 60°$). In contrast, at larger incidence angles ($\theta \geq 60°$) and HH polarization, breaking of waves dominates the radar return. Similar results are obtained at other radar wavelengths. As discussed in part 1, this higher sensitivity of HH radar cross section to wave breaking with respect to the VV polarization case, is responsible for the significant deviation of the polarization ratio from the Bragg scattering prediction.

[14] To apply the proposed model, we need to define the range of wave numbers involved in the different processes (the model is a three-scale model). We assume that the wave number K of the LW modulating the NRCS, is significantly smaller than both the wave numbers k_t defining the upper limit of tilting waves and the wave number k_{nb} which defines the upper limit of the range of breaking waves (i.e., $K \ll k_t, k_{nb}$). We also assume that the lower limit k_{mod} of the range of short waves, which experience modulations correlated with LW, is much larger than the LW wave number K ($k_{mod} = 10$ K). The smallest scale $k^{-1} = k_{br}^{-1}$ is responsible for the resonant Bragg scattering. Waves of the intermediate scales from k_{mod}^{-1} to $k_t^{-1} \approx k_{nb}^{-1}$ are responsible for the tilting of the Bragg waves and for the non-Bragg scattering.

[15] The standard procedure of linear decomposition of M_σ^p gives the following expression for the small disturbances of the NRCS caused by modulating LW, which in terms of the radar MTF M_σ^p reads:

$$M_\sigma^p = M_t^p + M_h^p \tag{13}$$

The first term M_t^p describes LW-induced variations in the NRCS due to changes of the local incidence angle (under the invariable wave properties providing the radar return). According to the accepted terminology, this term is attributed to the tilt part of the radar MTF. The second term M_h^p describes LW-induced variations of the NRCS caused by modulations of the surface waves of the intermediate scales providing both Bragg and non-Bragg scattering (under constant incidence angle). This part of the radar MTF is attributed to the so-called hydrodynamic MTF.

This representation of the radar MTF (for the real aperture radar) as sum of tilt and hydrodynamic MTF is the result of the linear decomposition of the NRCS on small variations caused by LW. The physical meaning of each of the radar MTF components is clear: M_t^p is due to the impact of varying local incidence, whereas M_h^p is related to the varying surface scattering features (independently on what concrete scattering mechanism occurs in reality). Below, within the frame of the proposed semiempirical NRCS model of part 1, we derive equations for the tilt and hydrodynamic parts of the radar MTF, and then compare the model predictions with measurements.

2.2. Tilt MTF

[16] If φ is the antenna direction, and LW are supposed to propagate along the x_1 axis, then the tilt MTF is defined as:

$$M_t^p = i\frac{1}{\sigma_0^p(\theta)}\frac{\partial\sigma_0^p(\theta)}{\partial\theta}\cos\varphi \tag{14}$$

Using (5) for the total NRCS with Bragg and non-Bragg components from (6) and (10) respectively, the tilt MTF is thus:

$$M_t^p = \left[(1-P^p)\left(M_{tb}^p + r_s M_{t2}^p\right) + P^p r_q M_{twb}\right]\cos\varphi \tag{15}$$

where P^p is the ratio of non-Bragg scattering to the total NRCS, M_{tb}^p is the tilt MTF for the pure Bragg scattering, M_{t2}^p is the contribution of the intermediate-scale tilting waves, M_{twb} is the tilt MTF for the non-Bragg scattering. These components are:

$$M_{tb}^p = i\frac{1}{\sigma_{0br}^p}\frac{\partial\sigma_{0br}^p}{\partial\theta} \tag{16}$$

$$M_{t2}^p = i\frac{g^p\overline{\nabla\zeta_i^2}}{1+g^p\overline{\nabla\zeta_i^2}}\frac{1}{g^p}\frac{\partial g^p}{\partial\theta} \tag{17}$$

$$M_{twb}^p = i\frac{1}{\sigma_{0wb}}\frac{\partial\sigma_{0wb}}{\partial\theta} \tag{18}$$

r_s is the ratio of the mean square slope contained in the range of intermediate scales ($k_{mod} < k < k_t$) to the mss $\nabla\zeta^2$ relative to the full range of tilting waves $k < k_t$, and r_q is the ratio of the fraction of the sea surface covered by enhanced roughness generated by breaking of waves of intermediate scales to the total q defined by (12). Note that the tilt MTF (as well as each of its components) is a pure imaginary number, whose phase is $+\pi/2$ or $-\pi/2$ depending on antenna direction.

[17] In Figure 2, the tilt MTF amplitude relative to the pure Bragg scattering model ((16), dotted lines), composite Bragg scattering model (sum of (16) and (17), dashed line) and total NRCS model ((15), solid lines) are shown as a function of incidence angle (conditions are wind speed 10 m/s, C-band, and upwind looking direction). Due to the small contribution of wave breaking to the NRCS at VV polarization (see Figure 1), M_t^{vv} is mainly defined by the pure Bragg scattering mechanism. Accounting for the tilting waves and non-Bragg scattering influences only slightly the tilt MTF at VV polarization. In contrast at

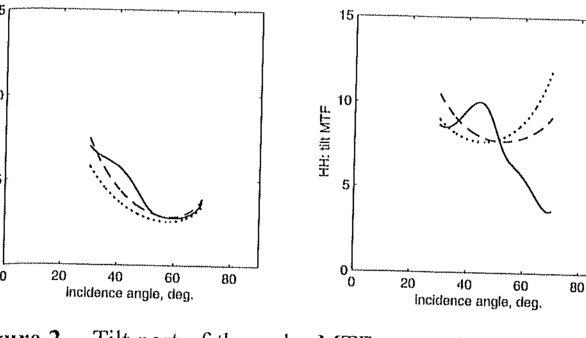

Figure 2. Tilt part of the radar MTF versus incident angle according to the pure Bragg model (dotted lines), the composite Bragg model (dashed lines), and the total scattering model (solid lines). Left panel is for VV polarization, and right panel is for HH polarization. Conditions: wind speed 10 m/s, C-band, upwind radar look direction.

HH polarization, the impact of tilting waves causes a significant deviation of the Bragg scattering tilt MTF from the pure Bragg tilt MTF. In addition, the influence of the non-Bragg scattering on the tilt MTF is very strong. The total tilt MTF M_t^{hh} is more or less close to M_{tb}^{hh} at moderate incidence angles (30°–45°). At larger incidence it significantly deviates from the Bragg MTF, and rapidly drops. Such a behavior is first explained by the fact that at large incidence angle) wave breaking dominates the NRCS (see Figure 1). In these conditions, the total tilt MTF is governed by M_{twb} given by (18), with (11) to express σ_{0wb}. Because at large incidence angle, σ_{0wb} is dominated by the second term of (11) which is a constant, M_{twb} and hence the total tilt MTF tends to zero at large θ.

[18] It is important to note that, according to (15), (16), (17), and (18) the tilt MTF is wind dependent. This is mainly due to the wind speed dependence of the ratio P^p of non-Bragg scattering to the total NRCS (see Figure 1 for C-band). Indeed, the tilt MTF for pure Bragg and non-Bragg scattering ((16) and (18)) do not depend on wind speed, and the dependence with wind speed of the tilting waves of the intermediate scale (in (17)) is relatively small.

2.3. Hydrodynamic Part of MTF

[19] According to the developed scattering model and to the linear decomposition of the surface NRCS, the hydrodynamic part of the radar MTF M_h is represented as a sum of three contributions related to the modulation of Bragg scattering waves, to the variation of the mean square slope of the tilting waves, and to wave breaking modulation.

[20] The Bragg part of hydrodynamic MTF is deduced from (6):

$$M_{hb} = M_{h0} + \frac{g^p \overline{\nabla\zeta^2}}{1 + g^p \overline{\nabla\zeta^2}} M_{hs} \qquad (19)$$

where $M_{h0} = \hat{\sigma}_{0br}/(\bar{\sigma}_{0br}KA)$ is associated with the modulation of Bragg scattering waves, and M_{hs} with the mean square slope modulation of the tilting waves of the intermediate scales. M_{h0} and M_{hs} can both be expressed in terms of the wave directional spectrum MTF: $M = \hat{B}(\mathbf{k})/(\bar{B}(\mathbf{k})KA)$. The pure Bragg contribution M_{h0} is defined via the folded spectrum $B_r(\mathbf{k}) = 1/2(B(\mathbf{k}) + B(-\mathbf{k}))$, and has the following form:

$$M_{h0}(\mathbf{k}_{br}) = 1/2\left(M(\mathbf{k}_{br})\frac{B(\mathbf{k}_{br})}{B_r(\mathbf{k}_{br})} + M(-\mathbf{k}_{br})\frac{B(-\mathbf{k}_{br})}{B_r(-\mathbf{k}_{br})}\right) \qquad (20)$$

M_{hs} follows from (9):

$$M_{hs} = \left(\overline{\nabla\zeta^2}\right)^{-1} \int_{k-\mathrm{mod}}^{k-t} k^{-2} B(\mathbf{k}) M(\mathbf{k}) d\mathbf{k} \qquad (21)$$

The modulation associated with the breaking waves at intermediate scales ($k_{mod} < k < k_{wb}$) follows (10) and (12) and can be written in terms of wave spectrum MTF as:

$$M_{hwb} = (n_g + 1) \frac{\int_{k-\mathrm{mod}}^{k-wb} k^{-1} \Lambda(\mathbf{k}) M(\mathbf{k}) d\mathbf{k}}{\int_{k<k-wb} k^{-1} \Lambda(\mathbf{k}) d\mathbf{k}} \qquad (22)$$

where n_g is related to the wind exponent m of the wave curvature spectrum $B(\mathbf{k})$ in the gravity range ($m = 2/n_g$) (see part 1). To obtain (22), we have used the parameterization introduced in part 1 for $\Lambda(\mathbf{k}) : \Lambda(\mathbf{k}) = 1/2k^{-1}(B(\mathbf{k})/\alpha)^{n_g+1}$ (α is a constant). (22) says that since wave breaking quantities are dependent on the spectral level, its modulation by LW results in wave breaking modulation. As it was shown in part 1, the main contribution to wave breaking comes from the shortest breaking waves. Hence, LWs (whose wavelengths are much longer than wavelengths of breaking waves) should effectively modulate the NRCS via wave breaking. Note that in (10), if we had kept the term describing the azimuth behavior of σ_{wb}, as done in part 1, an additional contribution should have been taken into account. However, this term is ($n_g + 1$) times smaller than the leading one. With $n_g = 5$, as stated in part 1, it is clear that this contribution can be omitted. Note also that with this value of $n_g = 5$, the magnitude of M_{hwb} is 6 times larger than the magnitude of the spectrum modulations.

[21] Finally, the hydrodynamic MTF contribution becomes:

$$M_h(k_r, \varphi) = (1 - P^p) M_{hb}(k_{br}, \varphi) + P^p M_{hwb}(k_r, \varphi) \qquad (23)$$

where P^p as before is the ratio of the non-Bragg scattering mechanism contribution to the total NRCS. Because P^p is larger for HH than for VV polarization (see Figure 1), the hydrodynamic MTF M_h for HH polarization is strongly enhanced by the non-Bragg contribution compared to the VV polarization case. Furthermore, because M_{hwb} is large, even a small value of P^p can explain a large value of M_h compared to it's Bragg component M_{hb}.

[22] To give a preliminary estimate of the role of non-Bragg scattering in the hydrodynamic MTF, let us consider the case of C-band radar with an incidence angle $\theta = 30°$ and a wind speed of 10 m/s. Under these conditions, the background NRCS model for VV polarization predicts $P^{vv} = \sigma_{wb}/\sigma_0{}^{vv} = 0.25$ (see Figure 1), and the tilting waves parameter $g^{vv}\overline{\nabla\zeta^2}$ is about 0.5. At HH polarization, $P^{hh} = \sigma_{wb}/\sigma_0{}^{hh} = 0.40$ (see Figure 1) and $g^{hh}\overline{\nabla\zeta^2} \approx 1.0$. If we assume that $M = 9/2$ at all k (value 9/2 is the k-exponent of the wave action spectrum $\partial \ln N/\partial \ln k \approx 9/2$ defining the

spectral MTF due to the straining; see (28) and (30), and discussion in section 3.2 after (45)), the estimates for the hydrodynamic part of the radar MTF for the Bragg scattering model are $M_{hb} = 6$ at VV polarization, and $M_{hb} = 6.7$ at HH polarization. When the non-Bragg scattering mechanism is taken into account, the total hydrodynamic part of the radar MTF gives $M_h = 11.2$ at VV, and $M_h = 14.8$ at HH. Two important conclusions can be given from these estimates. The first one is that non-Bragg scattering may increase the hydrodynamic part of the radar MTF by a factor of 2 in comparison with the "standard" Bragg scattering predictions. The second one is that this impact of non-Bragg scattering is larger for HH polarization. To explain the large magnitudes of the observed hydrodynamic part of the radar MTF in HH (compared to Bragg predictions), other authors [e.g., *Schroeder et al.*, 1986; *Hara and Plant*, 1994; *Romeiser et al.*, 1994] invoked a very strong surface wind stress modulation mechanism (with a normalized amplitude exceeding by a factor of 10 the LW steepness). However, the exact mechanism responsible for such strong wind stress was not described. Therefore, we believe that invoking non-Bragg scattering as done here is more adequate.

3. Modulations in the SW Spectrum

3.1. Governing Equations

[23] To complete the problem we need to describe the modulation of the short wind wave (SW) spectrum by the LW. To consistently describe both the background NRCS of the sea surface and its modulation by a LW, the modulations of SW are based on the same energy balance as used in part 1 for the wind wave spectrum. When the wave number k of the modulated SW is much larger than K (hence the SW group velocity is much less than the LW phase velocity), variations in the SW action spectrum $\tilde{N}$ are small (i.e., $\tilde{N}/N_0 \ll 1$), and the wave action balance equation reduces to [e.g., *Keller and Wright*, 1975; *Alpers and Hasselmann*, 1978]:

$$\frac{\partial \tilde{N}}{\partial t} - k_1 \frac{\partial u}{\partial x_1} \frac{\partial N}{\partial k_1} = \frac{\tilde{Q}}{\omega} \tag{24}$$

where N is the wave action ($N(\mathbf{k}) = \omega k^{-1} F(\mathbf{k})$, with ω the angular frequency of the waves), $\tilde{Q}$ is a small perturbation of the energy source Q. In the equilibrium range of the spectrum from very short capillaries to gravity waves this source has the form (see also part 1):

$$Q = \omega^3 k^{-5} \left[\beta_\nu(\mathbf{k}) B(\mathbf{k}) - B(\mathbf{k}) \left(\frac{B(\mathbf{k})}{\alpha} \right)^n + I_{pc}(\mathbf{k}) \right] \tag{25}$$

where $\beta_\nu = (\beta_0 - 4\nu k^2/\omega) \exp(-(\varphi - \varphi_w)^2)$ is the effective growth rate (ν is the water viscosity), $\beta_0 = C_\beta (u_*/c)^2$ is the wind growth rate in the wind direction (so that $\beta = \beta_0 \exp(-(\varphi - \varphi_w)^2)$ is the directional wind wave growth rate), u^* is the air friction velocity, φ_w is the direction of wind velocity, φ is the direction of the wave number vector $\mathbf{k}$, and ω is the wave frequency. In (25), the first term is the effective wind energy input, the second term describes the nonlinear energy losses which are provided (depending on spectral interval) either by wave breaking or resonant three-wave interactions, and the third term $I_{pc}(\mathbf{k})$ describes the generation of parasitic capillaries by short breaking gravity waves

$$I_{pc}(\mathbf{k}) = \hat{D}(\mathbf{k}_g) \phi(k_\gamma/k) \equiv B(\mathbf{k}_g) \left(B(\mathbf{k}_g)/\alpha \right)^{n(\mathbf{k}_g)} \phi(k_\gamma/k) \tag{26}$$

This energy source is effective in the capillary range (this is accounted for in the filter function $\phi(k_\gamma/k)$) and the generation of parasitic capillaries results in energy dissipation $D(\mathbf{k}_g)$ of gravity waves. In (26), $\hat{D}(\mathbf{k}_g) = \omega_g^{-3} k_g^5 D(\mathbf{k}_g)$ is the dimensionless dissipation of short gravity waves (with wave number k_g, and frequency $\omega_g = \omega(k_g)$) generating parasitic capillaries (with wave number k); wave numbers k and k_g are linked by $k k_g = k_\gamma^2$ (where $k_\gamma = (g/\gamma)^{1/2}$ is the wave number of the minimum phase velocity, γ is the surface tension, g is the acceleration of gravity). Expression for the small disturbances of the energy source can be found from (25):

$$\begin{aligned} \tilde{Q}/\omega = {} & \omega \overline{N} \left[\tilde{\beta} - (n\beta_\nu + (n+1)\beta_{pc}) \cdot \left(\frac{\tilde{B}(\mathbf{k})}{\overline{B}(\mathbf{k})} \right) \right. \\ & \left. + \beta_{pc} (n(\mathbf{k}_g) + 1) \cdot \left(\frac{\tilde{B}(\mathbf{k}_g)}{\overline{B}(\mathbf{k}_g)} \right) \right] \end{aligned} \tag{27}$$

where $\tilde{\beta}$ is a variation in the directional wind wave growth rate, $\beta_{pc} = I_{pc}(\mathbf{k})/B(\mathbf{k})$ is a parameter of the growth rate of parasitic capillaries, and $\overline{N}$ or $\overline{B}$ stands for the average of these variables over the LW.

[24] (24) and (27) can be easily solved. In terms of the MTF this solution is:

$$\begin{aligned} M(\mathbf{k}) = {} & -\left(\frac{1 - i\tau}{1 + \tau^2} \right) \frac{k_1}{\overline{N}(\mathbf{k})} \frac{\partial \overline{N}(\mathbf{k})}{\partial \mathbf{k}_1} + \frac{(\tau + i)}{1 + \tau^2} \\ & \cdot \left[2\tau_* M_* + \tau_{pc} (n(\mathbf{k}_g) + 1) M(\mathbf{k}_g) \right] \end{aligned} \tag{28}$$

where $\tau = (T\Omega)^{-1}$ is the dimensionless relaxation parameter of the spectrum, T the relaxation time defined as:

$$T^{-1} = \omega (n\beta_\nu + (n+1)\beta_{pc}) \tag{29}$$

$\tau_* = (\omega\beta/\Omega)$ and $\tau_{pc} = (\omega\beta_{pc}/\Omega)$ are the dimensionless wind growth rate, and dimensionless growth rate of parasitic capillaries, respectively, M_* is the MTF for the surface friction velocity. (28) describes the modulation of the wave spectrum B, resulting from the interaction of SW with LW orbital velocity (first term), from the wind surface stress (the second term), and from short gravity waves emitting parasitic capillaries (the third term, $M(\mathbf{k}_g)$ is the MTF of these gravity waves). The first term of (28) is the straining factor and can be rewritten as:

$$\frac{k_1}{N(k,\varphi)} \frac{\partial N(k,\varphi)}{\partial k_1} = \cos^2\varphi \frac{\partial \ln N}{\partial \ln k} - \sin\varphi \cos\varphi \frac{\partial \ln N}{\partial \varphi} \tag{30}$$

(28) predicts an asymptotic regime of SW modulations. If the relaxation time for a given spectral component is much larger than the period of LW (i.e., $\tau \ll 1$), then SWs interact with LW adiabatically (only the first term remains in (28))

and experience a simple straining with the increase of modulation on the LW crests. If LW runs in the crosswind direction, then SW modulations vanish. At high wind conditions (or for very short SW at moderate wind) the relaxation time may be much less than the period of LW (i.e., $\tau \gg 1$). Then SW modulations due to straining (first term in right-hand side of (28)) is negligible, and modulation of the wind surface stress is the only source of SW modulations. In this case, SW modulations are completely defined by the magnitude of the local surface stress variations, which result from dynamics of the airflow over the LW. As it follows from (28), spectral MTF in this case is $M(\mathbf{k}) \approx (2/n)M_*$, where $2/n$ is the wind exponent of the spectra. Well inside the capillary range, the mechanism of generation of parasitic capillaries dominates. Indeed, in this range the condition $\tau \gg 1$ is fulfilled at any LW wind conditions. Moreover; at low and moderate winds, viscous dissipation dominates the energy losses, the ratio τ_{pc}/τ is close to 1 so that the magnitude of the spectral MTF in the capillary range is $(n(k_g) + 1)$ greater than the MTF for the short gravity waves.

3.2. LW-Induced Surface Stress Modulations

[25] LW-induced variation of the wind surface stress can play an important role in the modulations of SWs. To describe the friction velocity MTF M in (28) we use the model of the turbulent airflow over LW developed by *Kudryavtsev et al.* [2001b] with some simplifications. In this model the turbulent airflow is divided in two parts: the outer region (OR) at $z > l$ (z is a distance from the wavy surface) and the inner region (IR) at $z < l$ (after the study of *Belcher and Hunt* [1993]). The scale of the IR l is defined as:

$$Kl = 2\kappa u*/|U - 1(l) - C| \tag{31}$$

where κ is the von Karman constant, C the LW phase velocity, and $\overline{U}_1(l)$ is the mean wind velocity along x_1 axis at $z = l$. In the OR, dynamics of the airflow undulations is closed to the inviscid one, and the wind velocity profile resulting from the solution of the vorticity equation is [see *Kudryavtsev et al.*, 2001b, equation (34)]

$$\hat{U}_1(z)/(KA) = \left(\overline{U}_1(z) - C\right)\exp(-Kz) + 2\left(u*/\kappa\right)\cos\varphi \cdot \int_z^{\infty} \exp(-Kz')d\ln z' \tag{32}$$

where $\hat{U}_1(z)$ is the amplitude of the LW-induced wind velocity variations, and $\overline{U_1}(z)$ the mean value of U_1 over a LW. In the OR the wave-induced wind velocity variations along the LW crest (in the direction of x_2 axis) vanish, i.e., $\hat{U}_2 = 0$.

[26] Inside the IR, the turbulent stress is in local balance with the wind velocity gradient:

$$u_*^2 = \kappa^2 z^2\left((\partial U_1/\partial/z)^2 + (\partial U_2/\partial/z)^2\right) \tag{33}$$

where wind velocity components U_i are the sum of the mean $\overline{U}_i$ and of the LW-induced variation $\tilde{U}_i$. To estimate the friction velocity MTF, we (unlike *Kudryavtsev et al.* [2001b]) use a schematic simplified description of the IR dynamics. We approximate the horizontal wind velocity variation inside the IR ($z_0 \le z \le l$) by a logarithmic profile. We also assume that the surface aerodynamic roughness along the LW surface can vary. Thus, in terms of harmonic amplitudes the LW-induced variation of wind velocity inside the IR is:

$$\hat{U}_1(z) = \left[\hat{u}_0 - \left(\bar{u}*/\kappa\right)\cos\varphi(\hat{z}_0/\bar{z}_0)\right] + c_u\ln(z/\bar{z}_0) \tag{34}$$

where $\hat{u}_0$ = (KA)C is the amplitude of the LW orbital velocity, c_u is a constant defined so as to patch the wind velocity profiles inside the OR (given by (32)) and the IR (given by (34)) at $z = l$.

$$c_u = \left(\Delta\hat{U}_1 + \left(\bar{u}*/\kappa\right)\cos\varphi(\hat{z}_0/\bar{z}_0)\right)/\ln(l/z_0), \tag{35}$$

where $\Delta\hat{U}_1 = \hat{U}_1(l) - \hat{u}_0$ is the wind velocity drop over the IR.

[27] Thus, by the combined effects of the variation along the LW of the wind profile and of the roughness length, one obtains the following expression for the MTF M_* of the wave spectrum, due to friction velocity variations:

$$M* \equiv \hat{u}*/\left(\bar{u}*KA\right) = \cos^2\varphi[M_{\Delta U} + \ln^{-1}(l/\bar{z}_0)M_{z0}] \tag{36}$$

where $M_{\Delta U} = \Delta\hat{U}_1/(KA\hat{U}_1)$ is the normalized amplitude of the LW-induced horizontal velocity drop over the IR:

$$M_{\Delta U} = 1 - 2C/U_1(l) + 2\ln^{-1}(l/\bar{z}_0)\cdot\int_{Kl}^{\infty}\exp(-Kz')d\ln Kz' \tag{37}$$

(36) takes into account variations along the LW of the aerodynamic roughness ż0 (second term) as well as variations of the wind profile (first term).

[28] Taking into account the modulations of z_0 as just proposed, means that we are now dealing with the wind over waves coupling. Indeed, variations of the aerodynamic roughness length z_0 results from the modulations of the SW. Form drag of the sea surface is supported by momentum flux to the "regular" surface waves, and by momentum flux due to the airflow separation from breaking waves [*Kudryavtsev and Makin*, 2002]. At moderate and strong wind, the drag of the sea surface is almost provided by the form drag. Thus, SW modulations influence the sea surface aerodynamic roughness, which according to (36) affects the surface stress variations, which in turn stimulate SW modulations (second term in (28). This constitutes the so-called feed back mechanism existing in the coupled system "SW turbulent airflow" over LW. This problem has been recently analyzed in detail by *Kudryavtsev and Makin* [2002]. Including the complete theory is out of the scope of the present application to the radar MTF problem. So, we propose an alternative, which is based on the same physical basis, but which uses a semiempirical approach to describe the coupling.

[29] In terms of the sea surface roughness scale form drag can be expressed as

$$z_0 = a_\nu\nu_a/u* + \int\Phi(B)d\mathbf{k} \tag{38}$$

where the first term is associated to viscous drag and the second term is associated to the impact of momentum flux to waves and to the airflow separation on the sea surface drag. We express the second term as an unknown functional of the wave spectrum $B(\mathbf{k})$. Then, variation of the roughness scale z_0 due to the SW spectrum modulation reads (in terms of MTF):

$$M_{z0} \approx \bar{z}_0^{-1} \int \bar{B}\Phi'_B M d\mathbf{k} \equiv \bar{z}_0^{-1} \langle M \rangle \int \bar{B}\Phi'_B d\mathbf{k} \qquad (39)$$

where $\Phi'_B = \partial\Phi/\partial B$, and $\langle M \rangle$ is the average MTF over the wave numbers k of the wave spectrum B weighted over the function $B\Phi'_B$. To derive M_{z_0} according to (39) we omitted the variation in u_* (associated with the first term of (38)) caused by SW modulations via z_0); the contribution of this term to M_{z_0} is $\ln(l/\bar{z}_0)$ times less than the impact of the second term in (38). To eliminate the unknown functional $\int \Phi'_B d\mathbf{k}$, we introduce the wind exponent m_{z0} of the roughness scale z_0:

$$m_{z0} = (u_*/z_0)(\partial z_0/\partial u_*) \qquad (40)$$

which can be determined from (38) as:

$$m_{z0} z_0 = -a_\nu \nu_a/u_* + u_* \int \frac{\partial\Phi}{\partial u_*} d\mathbf{k} = -a_\nu \nu_a/u_* + \int m\bar{B}\Phi'_B d\mathbf{k} \qquad (41)$$

where the term $m = \partial \ln \overline{B}/\partial \ln u_*$ is the wind exponent of the wave spectrum. Then the unknown functional is:

$$\int \bar{B}\Phi'_B d\mathbf{k} = \frac{m_{z_0} z_0 + a_\nu \nu_a/u_*}{\langle m \rangle} \qquad (42)$$

where $\langle m \rangle$ is the average of m over the wave numbers k, weighted by function $\overline{B}\Phi'_B$ Thus, from (39) and (42), we obtain the MTF of z_0 as:

$$M_{z-0} = \frac{\langle M \rangle}{\bar{z}_0 \langle m \rangle} \left(m_{z_0} z_0 + \frac{a_\nu \nu A a}{u_*} \right) \qquad (43)$$

The advantage of this equation for the roughness scale MTF (in comparison with (39)) is that the problem now is reduced to the determination of an explicit relation for z_0 and its wind exponent. *Kudryavtsev and Makin* [2002] showed that wind over wave coupling theory gives the aerodynamic roughness scale which at moderate and high winds is close to Charnock relation and at low winds is close to aerodynamically smooth surface. The latter fact is accounted for in (38). Hence, to assess z_0 and m_{z_0} in (43), we can simply use a semiempirical relation for the roughness scale. As in part 1, we specify z_0 as: $z_0 = a_\nu \nu_a/u_* + a_* u_*^2/g$ where parameter a_ν is a constant ($a_\nu = 0.1$) and a_* is the Charnock parameter ($a^* = 0.018$). Then, (43) reads:

$$M_{z0} = \frac{2\langle M \rangle}{\langle m \rangle} \frac{a_* u_*^2/g}{\left(a_\nu \nu_a/u_* + a_* u_*^2/g\right)} \qquad (44)$$

To prescribe the mean spectral wind exponent $\langle m \rangle$ in (44), we recall that the roughness scale is defined by two components of the form drag: momentum flux to the waves and the airflow separation. The former is supported by SW in a wide wave number range from capillary gravity to gravity waves down to the energy containing waves. One may anticipate that weighted wind exponent of these waves is close to that typical for the mean square slope of the sea surface, which depends linearly on wind speed. Breaking waves supporting the airflow separation are waves from equilibrium gravity interval where wind exponent is $2/n_g$. Then fixing $\langle m \rangle$ as the mean value of the exponent relative to the two regimes, we have $\langle m \rangle \approx (2 + n_g)/(2n_g)$. To estimate $\langle M \rangle$ we suggest that the main contribution to the form drag modulations by LW comes from the SW which experience adiabatic modulations by LW (straining mechanism dominates SW modulations, and enhancement of SW occur on the LW crests). This suggestion is a reliable one for the wave breaking (see Figure 4 below), and is very plausible for SWs supporting wave momentum flux. Then $\langle M \rangle$ is estimated from (28) and (30) as $\langle M \rangle \approx \partial \ln N/\partial \ln k$. From the definition of N ($N = F\,\omega/k$) and the fact that the curvature spectrum B is constant in the gravity and capillary gravity range (see part 1), this gives $\langle M \rangle \approx 9/2$. Finally, the roughness scale MTF M_{z0} reads:

$$M_{z0} = \frac{18 n_g}{2 + n_g} \cdot \frac{a_* u_*^2/g}{\left(a_\nu \nu_a/u_* + a_* u^2/g\right)} \qquad (45)$$

With the value of n_g discussed in part 1 ($n_g = 5$), this equation predicts a roughness scale MTF $M_{z0} \approx 13$ at moderate and high winds. As a consequence of the assumption that SW supporting form drag is modulated adiabatically , enhancement of z_0 occurs on the LW crest. These results are very close to the calculations resulting from the full coupled model of SWs and the airflow over LW developed by *Kudryavtsev and Makin* [2002, Figures 5 and 6]. According to (45), at low wind, roughness scale modulations vanish. This is simple but remarkable physical property of (45) indicating that the weaker is the form drag, the weaker is the impact of aerodynamic roughness on the LW-induced stress modulations.

3.3. Model Results for the Modulation of the Wave Spectrum and of the Wave Breaking

[30] Figure 3 shows for different conditions the amplitude and phase of the SW spectrum modulation M, calculated from (28) where all the terms have now been described. 3 cases of wave development are considered under a 10 m s^{-1} wind speed: an "old sea" case with a LW of inverse wave age $U_{10}/C = 0.5$ (upper panels), a fully developed wind-sea $U_{10}/C = 1$ (middle panels), and a young wind-sea $U_{10}/C = 3$ (lower panels). Dashed lines show the model calculations when surface stress variations and generation of parasitic capillaries are not accounted for , while the solid lines are for the full model. In all cases the longest modulated SWs (k < 100 rad/m) show a behavior typical of adiabatic modulations (the relaxation parameter τ is small), with $|M| \approx 9/2$ and enhancement of the SW energy is located on the crest of LW. In this range, there is no impact of stress modulation whatever is the wave age. For SWs with a large relaxation parameter τ but outside the capillary range, (100 < k < 740 rad/m), variations of the wind surface stress significantly affects the modulation in the case of swell ($U_{10}/C = 0.5$) and young sea state ($U_{10}/C = 3$). In the former

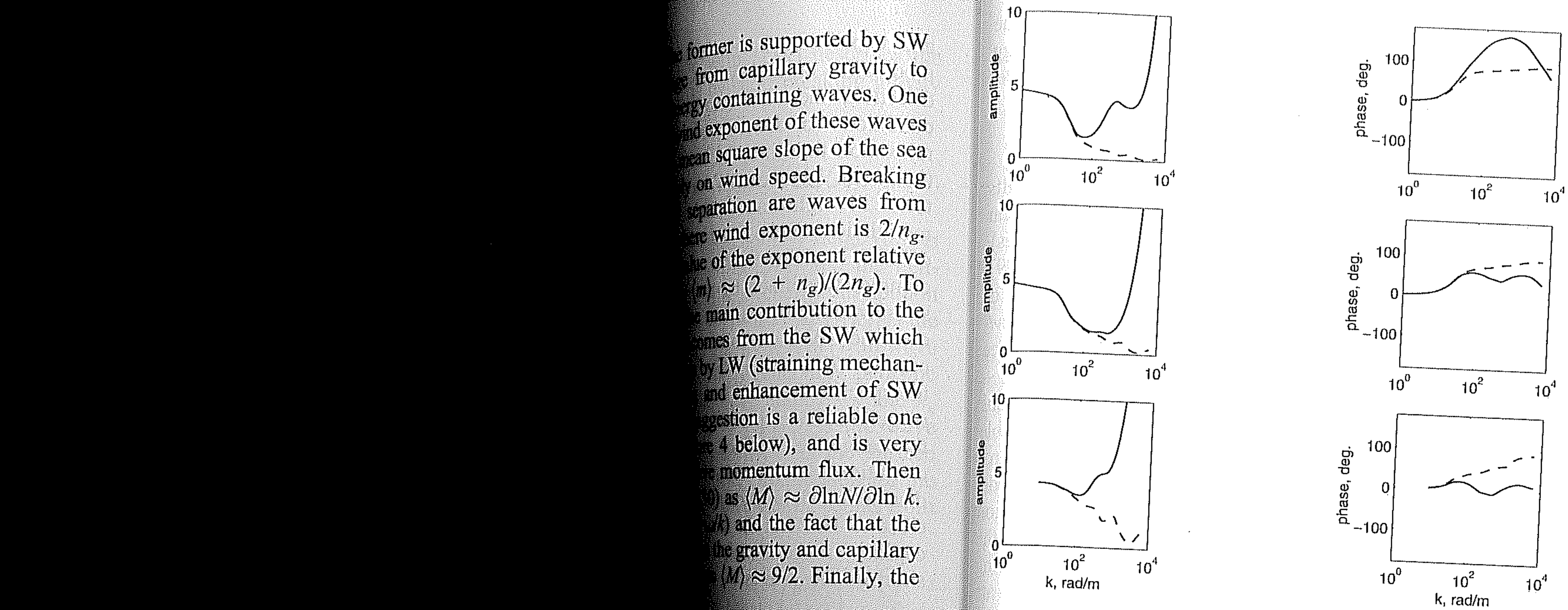

Figure 3. Amplitude (left) and phase (right) of the modulations of the SW spectrum by LW of inverse wave age U_{10}/C = 0.5 (upper panels), U_{10}/C = 1.0 (middle panels), and U_{10}/C = 3.0 (lower panels) at wind speed U_{10} = 10 m/s. Dashed lines show the model results when wind velocity variations and generation of parasitic capillaries are not taken into account, whereas solid lines are for the full model.

case, the surface stress is increased in the vicinity of LW trough so that the phase of the capillary gravity waves (whose modulations are dominated by the surface wind stress) is shifted toward the LW trough. In the latter case the surface stress is increased on the LW crest, thus capillary gravity waves are enhanced on the LW crest. For the case U_{10}/C = 1.0, the effect of wind stress modulation is weak in the range (100 < k < 740 rad/m). Finally, another noticeable result of the model calculations is the large modulations in the capillary range ($k > 2k_\gamma$ = 740 rad/m). As it was discussed above, the amplitude of the MTF of capillary waves is amplified by a factor $(n_g(k_\gamma) + 1)$ with respect to the amplitude of the MTF of the carrying short gravity waves. This is so-called mechanism of a cascade modulation of the parasitic capillaries.

[31] From the model estimates for the modulation of wave spectrum (M) the wave breaking MTF (M_{hwb}) (22) can also be calculated. Results for various winds and LW wave numbers are shown in Figure 4 (dotted lines for K = 0.025 rad/m, solid lines for K = 0.1 rad/m, dashed-dotted lines for K = 0.4 rad/m). Calculations were performed according to (22) where the upper limit of integration k_{wb} was fixed to $2\pi/0.3$ rad/m. Experimental estimates of MTF for the white cap coverage obtained by *Dulov et al.* [2002] are shown in Figure 4 as open circles with error bars. They correspond to a modulating LW wave number in the range 0.08 rad/m to 0.25 rad/m. In spite of a large scatter (error bars correspond to 95% confidence level), the measurements exhibit very strong wave breaking modulations (averaged MTF amplitude is 22) with enhancement on the crests of modulating LWs. Model calculations also predict enhancement of wave breaking in the vicinity of LW crest with large amplitudes for the MTF. Although the model predictions slightly underestimate the observations, the important conclusion is that modulations of wave breaking can be strong enough to significantly affect the radar MTF.

4. Model Results for the Hydrodynamic Components of the Radar MTF

[32] As described above, the hydrodynamic part of the radar MTF is defined by (23) where the Bragg scattering contribution (first term, M_{hb}) results from (19), (20), and (21), and the non-Bragg scattering contribution M_{hwb} results from (22). The SW spectrum modulation is defined by (28). The amplitude and phase of the different modulating processes contributing to these terms are presented in Figure 5 as a function of wind speed: straining of Bragg waves (open circles), effect of the wind surface stress (open triangles), modulation of tilting waves (crosses) and wave breaking (stars). For Figure 5, we consider conditions of Bragg waves corresponding to a C-band radar looking at an incidence angle of 45°, and a modulating LW with frequency of 0.15 Hz.

[33] The first remarkable result which appears in Figure 5 is that at all wind speeds, the amplitude of the wave breaking component of the hydrodynamic MTF (lines marked by stars) is larger than the amplitudes associated with the other processes. This component provides a maximum of radar modulation occurring near the LW crests (see the right-hand panel in Figure 5). As it was mentioned above, although the contribution of breaking waves to the total NRCS is not dominant (at least at VV polarization, and in the range 40° ≤ θ ≤ 60° at HH polarization, see Figure 1), the strong modulations of breaking can significantly contribute to the hydrodynamic part of the radar MTF. Effect of the straining of Bragg waves (lines marked by open circles) is large at low wind speeds only (U < 6–7 m/s). Amplitude of wind stress modulations (lines marked by triangles) is quite large at small wind speed (U < 6–7 m/s), shows a minimum value for intermediate wind values (6–7 to 11 m/s) and then increases slightly again at large wind. Maximum of wind stress variations occur in the LW troughs (respectively on the LW crests) for wind speed smaller (respectively larger)

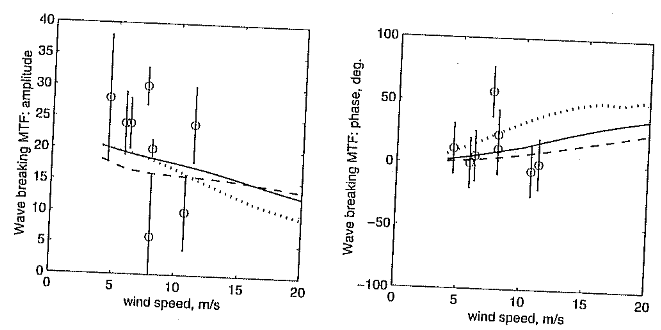

Figure 4. Amplitude and phase of the wave breaking MTF versus wind speed. Open circles and error bars are data from the study of *Dulov et al.* [2002]. Model calculations are shown by dotted lines (LW wave number 0.025 rad/m), solid lines (LW wave number 0.1 rad/m), and dashed lines (LW wave number 0.4 rad/m).

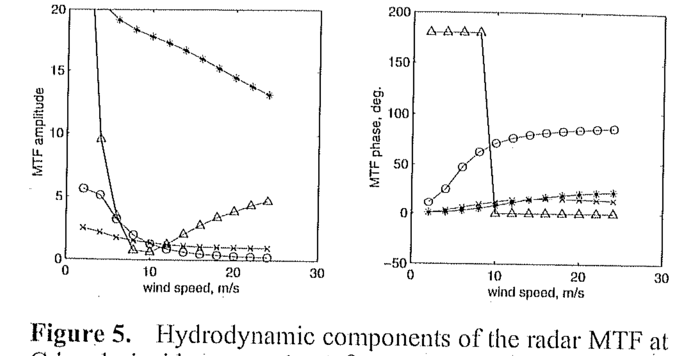

Figure 5. Hydrodynamic components of the radar MTF at C-band, incidence angle 45°. The left panel is for the amplitude of the MTF, and the right panel is for the phase of the MTF. Open circles correspond to the term due to Bragg waves when accounting for the straining effect only. Open triangles correspond to the term due to wind surface stress modulations. Stars correspond to the term due to wave breaking. Crosses correspond to the term due to the mean square slope of tilting waves.

than 10 m/s. Wind stress can significantly affect Bragg waves resulting in a similar behavior of the Bragg waves along the LW. This result partly confirms the explanation proposed by *Romeiser et al.* [1994], *Hara and Plant* [1994], and *Schmidt et al.* [1995], who suggested that strong amplification of the wind stress over LW crests is the source of Bragg waves modulations. However, our results indicate that amplification of wind stress over LW crest can occur only at winds exceeding 10 m/s. Modulation of the mean square slope of the intermediate-scale tilting waves (lines marked by crosses) is small (amplitude is about 2). The slope of these tilting waves increases on the LW crests, but the small amplitude of their modulation does not significantly affect the hydrodynamic MTF.

[34] Results discussed here are qualitatively similar for other radar wavelength conditions (from Ka-band to C-band) and other LW frequencies. In contrast, results at L-band are significantly different as explained in section 5.4 below.

5. Comparison With Radar Observations

[35] In this section, we compare the model predictions of the hydrodynamic MTF with radar observations in a wide range of radar frequencies from L to Ka band. Except for the RESSAC C-band data, the hydrodynamic MTF has been estimated as a residual part between the total radar MTF and the tilt MTF corresponding to the pure Bragg scattering model. For the RESSAC data, the tilt contribution is estimated by (14). As discussed above, the "real" tilt MTF differs from the pure Bragg tilt one. However, at moderate incidence angle, this difference is not so significant and we can identify our model hydrodynamic MTF with the definition used in the experimental studies.

[36] Figures 6–10 show the model-derived and observed amplitudes and phases of the hydrodynamic MTF as a function of wind speed for Ka, X, C, and L bands at VV and HH polarizations and for an incidence angle 45°. For each simulation, wave and wind conditions have been chosen in accordance with the observations. To emphasize the role of various scattering mechanisms, we show the MTF for pure Bragg model (dashed lines), composite Bragg scattering model (dotted lines), and for the total model accounting for the non-Bragg scattering (solid lines).

5.1. Comparison at Ka-Band

[37] Figure 6 shows the comparison with results obtained at Ka-band by *Grodsky et al.* [1999] (star symbols) and by *Kudryavtsev et al.* [2001a] (open circles). Conditions of observations are: for *Grodsky et al.* [1999], radar wavelength 1.2 cm, incidence angle 45°, range of modulating LW frequencies 0.15 ÷ 0.4 Hz; for *Kudryavtsev et al.* [2001a], radar wavelength 0.8 cm, incidence angle 45°, range of modulating LW frequencies 0.15 ÷ 0.35 Hz. For both data sets, bars indicate standard deviations of the estimates from their mean value. The first remarkable features is that the experimental amplitude of the hydrodynamic MTF increases rapidly for decreasing wind speeds, and the second feature is that $|M_h|$ at HH polarization exceeds $|M_h|$ at VV polarization. Also, according to the experimental results, enhancement of the backscattering occurs in the vicinity of the LW crests. These features are well known and have been previously mentioned in studies on the MTF problem [e.g., *Hara and Plant*, 1994].

[38] Model calculations (lines) were performed for the radar wavelength of 1 cm and for a 0.25 Hz frequency of modulating LW (which is a mean for the range of observed LW frequencies). In this case the Bragg scattering waves are in the range of parasitic capillaries (the Bragg wavelength is 0.7 cm). Figure 6 also shows that the hydrodynamic part of the radar MTF according to pure Bragg and composite Bragg scattering models are very close. It means that the contribution associated with the intermediate scale is small. At VV polarization, the model calculations with the Bragg model reproduces reasonably well the observations for both amplitude and phase of the MTF. As it was discussed above, a large modulation amplitude in the capillary range occurs, due to the mechanism of generation of parasitic capillaries. At HH polarization, the Bragg model underestimates the observed MTF amplitude. Accounting for the non-Bragg scattering mechanism (solid lines) increases the amplitudes of the hydrodynamics MTF, improving the agreement between model and observations. At high winds, the ratio of non-Bragg scattering σ_{wb} to the total NRCS σ_0^p at VV polarization is $\sigma_{wb}/\sigma_0^{vv} = 0.2$ while at HH polarization it is $\sigma_{wb}/\sigma_0^{hh} = 0.5$. Hence the increased role of the non-Bragg scattering on HH polarization and the large amplitude of wave breaking modulation result in (according to (23)) the larger amplitudes of the hydrodynamic MTF in comparison to VV polarization. Since the main factors governing hydrodynamic MTF (wave breaking and surface stress) (see Figure 5) are enhanced on the LW crest, the phase of the hydrodynamic MTF is close to zero.

5.2. Comparison at X-Band

[39] Figure 7 shows model and observed hydrodynamic MTF relating to X-band. Experimental data are given by *Hara and Plant* [1994] (open circles) and *Schmidt et al.* [1995] (plus symbols). Similarly to the Ka-band case, the amplitude of the observed hydrodynamic MTF increases when wind speed decreases, (for wind speed smaller than about 7–8 m/s) and $|M_h|$ at HH polarization is higher than at

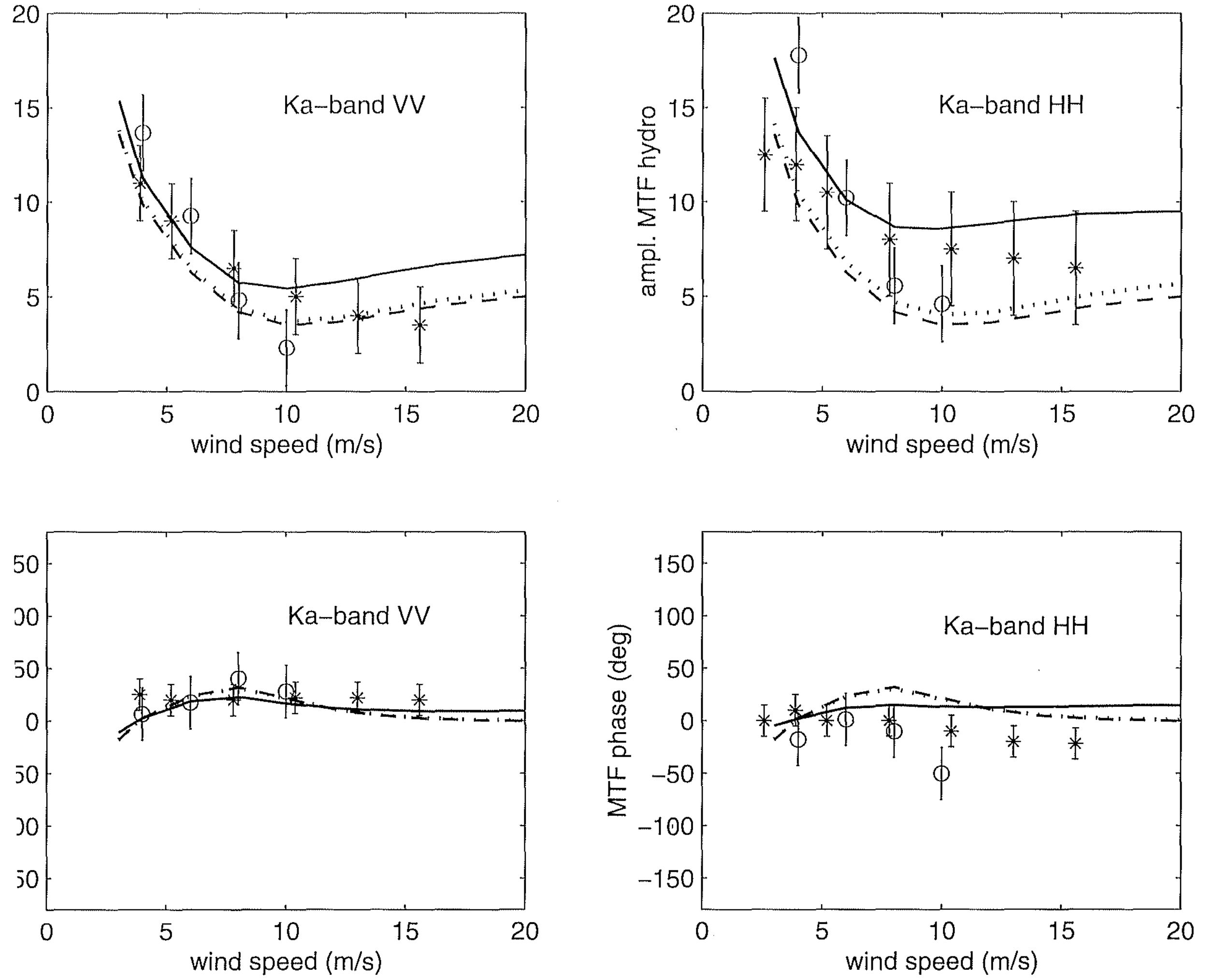

Figure 6. Amplitude (top panels) and phase (bottom panels) of the hydrodynamic part of the radar MTF versus wind speed for K-band at incidence angle 45°. Left side panels are for VV polarization, and right side panels are for HH polarization. Open circles with bars are measurements by *Kudryavtsev et al.* [2001a] (radar wavelength 0.8 cm, LW frequencies of 0.15–0.35 Hz). Stars with bars are measurements by *Grodsky et al.* [1999] (radar wavelength 1.2 cm, LW frequencies of 0.2–0.4 Hz). Model calculations of the hydrodynamic part of the radar MTF are for a radar wavelength of 1.0 cm and for a LW frequency of 0.25 Hz. They are shown by dashed lines (pure Bragg model), dotted lines (composite Bragg model), and solid lines (full model accounting wave breaking modulation). Conditions: Upwind radar look direction, LW aligned with the wind.

is is even more apparent than at Ka-band. At e and high winds, the amplitude of hydrodynamic ır HH polarization is approximately twice higher ıt at VV polarization. This fact has been often ed in radar MTF studies, but no explanation was ı far.

.s well as for Ka-band model calculations of $|M_h|$ n the Bragg scattering theory do not demonstrate erence between pure Bragg and composite models. ion of Bragg waves at low winds is caused by the straining mechanism (when $M \approx \partial \ln N/\partial \ln k$, see nd their large amplitudes ($|M_{hb}| \approx 5 - 7$) are d by the sharp drop of the spectrum toward higher ımbers (see part 1, Figure 4). At higher winds 10 m/s) Bragg waves modulations are suppressed vind, and then the MTF amplitude increases with wind speed due to the dominating action of the wind surface stress (see Figure 5), but this increase is weak. At VV polarization, the Bragg model in overall agrees with the observation predicting correctly the MTF amplitude and phase. The model confirms the suggestion given by *Hara and Plant* [1994] and *Schmidt et al.* [1995] that at high winds the modulation of Bragg waves is governed by the wind surface stress. However, model predictions based on the Bragg theory apparently contradict the observations obtained for HH polarization. For HH polarization, the fraction of the non-Bragg scattering in the total NRCS is $\sigma_{wb}/\sigma_0^{hh} = 0.52$ while for VV polarization it is $\sigma_{wb}/\sigma_0^{vv} = 0.22$. Model calculations of $|M_h|$ are then found to be in better agreement with the measurements when the non-Bragg scattering are accounted for. They correctly predict the order of magnitude of $|M_h|$, explain the observed

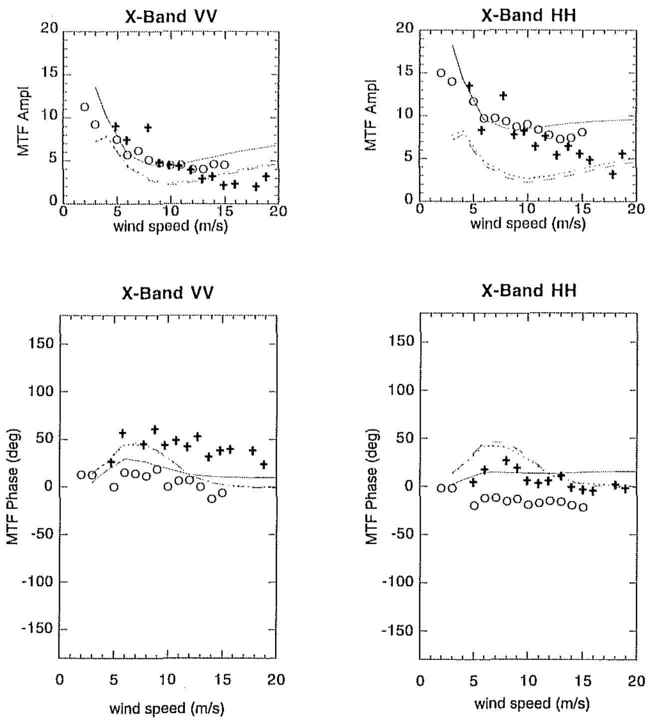

Figure 7. Amplitude (top panels) and phase (bottom panels) of the hydrodynamic part of the radar MTF versus wind speed for X-band at incidence angle 45°. Left side panels are for VV polarization, and right side panels are for and HH polarization. Open circles are data from the study of *Hara and Plant* [1994] (LW frequencies are 0.25 ÷ 0.31 Hz). Plus symbols are measurements of *Schmidt et al.* [1995] (LW frequency is 0.15 Hz). Model calculations for a LW frequency of 0.2 Hz are shown by dashed lines (pure Bragg model), dotted lines (composite Bragg model), and solid lines (full model accounting wave breaking modulation). Conditions: Upwind radar look direction, LW aligned with the wind.

difference between hydrodynamic MTF extracted from VV and HH data, and give a phase of the MTF closer to the observations.

5.3. Comparison at C-Band

[41] Model and observed estimates of the hydrodynamic MTF at C-band are shown in Figure 8. Data plotted in Figure 8 as plus symbols, correspond to the data of *Schmidt et al.* [1995]. As for the Ka and X band cases, observed amplitudes of the hydrodynamic MTF at HH polarization exceed the amplitudes obtained at VV one. For both polarizations the MTF enhancement of the sea surface scattering features occur on the LW crests. Model calculations based on the Bragg scattering theory significantly underestimate the observed $|M_h^p|$, and there is a discrepancy between model and observed MTF phases, which is the most apparent at HH polarization. Accounting for the modulation of wave breaking significantly affects the radar hydrodynamic modulation with respect to the Bragg case, with an increase of the amplitude (mainly in HH polarization) and a shift of its phase toward the crest of modulating LW. Although the full model underestimates the observed amplitudes of the MTF at low and moderate winds, it is in better agreement with the measurements than are the two-scale or pure Bragg models. Moreover, only the full model gives a phase in HH polarization consistent with the measurements.

[42] A further comparison between model and observations at C-band is given in Figure 9, with data from the airborne RESSAC radar collected during the FETCH experiment. We recall that RESSAC is an airborne FM/CW radar [*Hauser et al.*, 1992]. It operates at C-band (5.35 GHz) and HH polarization. The range resolution is 1.56 m. In its nominal mode, the radar beam sweeps the sea surface over the range of incidence angles $7° < \theta < 21°$, and scans over 360° in azimuth. Directional spectra are derived by analyzing in each azimuth direction, the modulations of radar cross section within the footprint (about 1500 × 400 m). In this range of incidence ($7° < \theta < 21°$), it can be assumed that the radar MTF is dominated by the tilt term, so that the spectrum of modulations (corrected for speckle noise) is linearly related to the slope spectrum of the waves (for wavelength longer than about 30 m). The tilt MTF is derived by applying (14) to the radar observations, dropping the cos φ term. During the FETCH experiment, RESSAC was also operated in a second mode to observe the surface in the incidence range $27° < \theta < 41°$: the antenna was fixed on one side of the airplane while this latter was performing circles with a roll of about 20°. By combining these two different modes of operation, *Hauser and Caudal* [1996] developed a method to estimate the hydrodynamic MTF near 30° incidence angle. The total MTF is estimated at

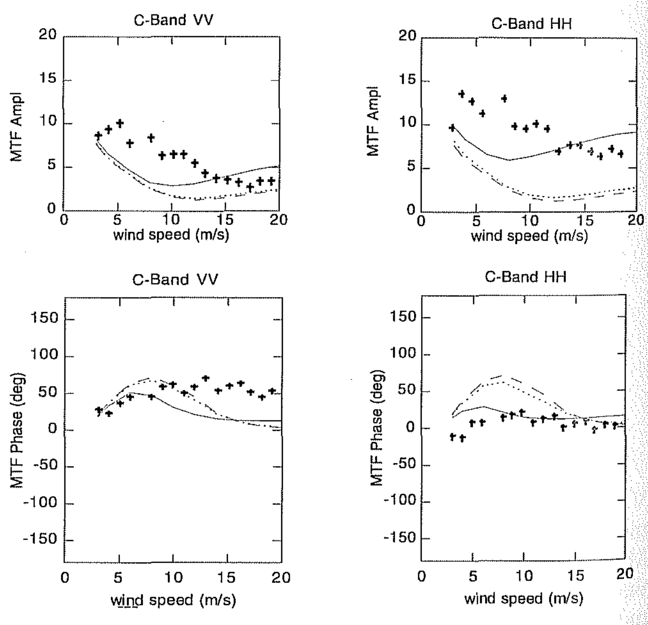

Figure 8. Amplitude (top panels) and phase (bottom panels) of the hydrodynamic part of the radar MTF versus wind speed for C-Band at incidence angle 45°. Left side panels are for VV polarization, and right side panels are for and HH polarization. Plus symbols are measurements by *Schmidt et al.* [1995] (LW frequency is 0.15 Hz). Model calculations for a LW frequency of 0.15 Hz are shown by dashed lines (pure Bragg model), dotted lines (composite Bragg model), and solid lines (total model accounting wave breaking modulation). Conditions: Upwind radar look direction, LW aligned with the wind.

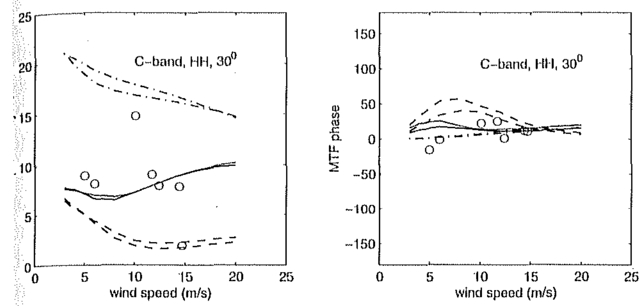

'igure 9. Amplitude (left panel) and phase (right panel) of ıe hydrodynamic part of the radar MTF versus wind speed C-band, HH polarization, incidence angle 30°). Open ircles are results obtained from the FETCH experiment.)ashed lines are Bragg scattering model predictions.)ashed-dotted lines are "pure" non-Bragg scattering model redictions. Solid lines are model predictions according to ıe total MTF model. Lines of the same style show model alculations for LW with wave numbers 0.08 and 0.15 rad/ ı. This was the range of LW wave numbers observed for ıis data set of the FETCH experiment.

ıcidence 30° from the ratio of the radar modulation pectrum to the directional wave slope spectrum (derived om the first mode of operation). By combining estimates f this total MTF in opposite directions (at φ and $\varphi + \pi$), ith the tilt MTF estimated at 30°, it was shown than the nplitude and phase of the hydrodynamic modulation in ıch look direction can be estimated. Results obtained from .is method applied to the FETCH data set are presented in igure 9, together with the model results.

[43] Model calculations were performed with LWs of ave numbers 0.08 rad/m and 0.15 rad/m (solid lines),)rresponding to the mean conditions of the RESSAC)servations. Only data for which in situ wind measure- ents (from buoy or ship) were available are displayed. hese reasons explain the low number of RESSAC data in gure 9. For the MTF amplitudes (left panel), the RESSAC ıta (open circles) exhibit a set of points with MTFs :tween 8 and 10, as well as two data points with MTF ' 15 and 2, respectively, both corresponding to very ısteady situations (both cases correspond to situations here a sudden large increase of wind speed occurred less an 2 hours before observation; they also correspond to the 'o data points with highest $\sigma_{0up}^{hh}/\sigma_{0cross}^{hh}$ and $\sigma_{0up}^{hh}/\sigma_{0down}^{hh}$ tios in Figure 15 of part 1). It appears clearly that the pure :agg model (dashed lines) underestimates the amplitudes)served by RESSAC. On the contrary, the pure non-Bragg attering model (dotted lines) gives much higher values etween 15 and 20). The full MTF model (solid lines) ıtained by combining both processes, predicts values in)ser agreement with the RESSAC data.

[44] For the hydrodynamic MTF phases (right panel of gure 9), we notice again that the full model (including non :agg effects) predicts phase angles between 0 and 20°, in reement with RESSAC observations, while the pure :agg model would predict a phase up to 60°.

4. Comparison at L-Band

[45] Figure 10 shows the hydrodynamic MTF at L-band. ; in Figure 8, the data used in the comparison are from the study of *Schmidt et al.* [1995]. Compared to the previous cases (higher radar frequencies) the observed amplitude of $|M_h|$ shows a weaker wind speed dependence, and a magnitude, which is approximately the same for both VV and HH polarizations. Model calculations shown in this figure are dominated by the straining mechanism. *Hara and Plant* [1994] also concluded that at L-band (MARSEN L-band data), the hydrodynamic MTF is primary due to the straining by LW orbital velocities except perhaps at very high winds. In contrast to the previous cases, the role of modulations of wave breaking is not significant. Contribution of the non-Bragg scattering to the total NRCS at L-band for a 20 m/s wind speed is $\sigma_{wb}/\sigma_0^{vv} = 0.09$ at VV and $\sigma wb/\sigma_0^{hh} = 0.30$ at HH polarization. For lower winds, these contributions decrease. This explains why the Bragg MTF model predictions are close to the total MTF one (except at high winds for HH polarization). The observed MTF amplitude systematically exceeds the model predictions. This is the only case where we do not get a satisfactory agreement between model and observations. We emphasize here that the observed amplitudes of the hydrodynamic part of the radar MTF at L-band are 1.5–2 times larger than the upper limit $\approx 9/2$ for SW modulation due to their straining by LW. Since straining is the only possible mechanism (because L-band Bragg waves are too "inertial" to be affected by the wind surface stress along the LW profile), it is hardly believable that the observed L-band hydrodynamic radar MTF amplitudes relate to any SW modulation mechanism. The reason of such large observed amplitude is not clear for us. A plausible explanation is given in below in section 5.5.

5.5. Summary and Discussion

[46] To summarize the results of this section we conclude that the hydrodynamic MTF based on the Bragg

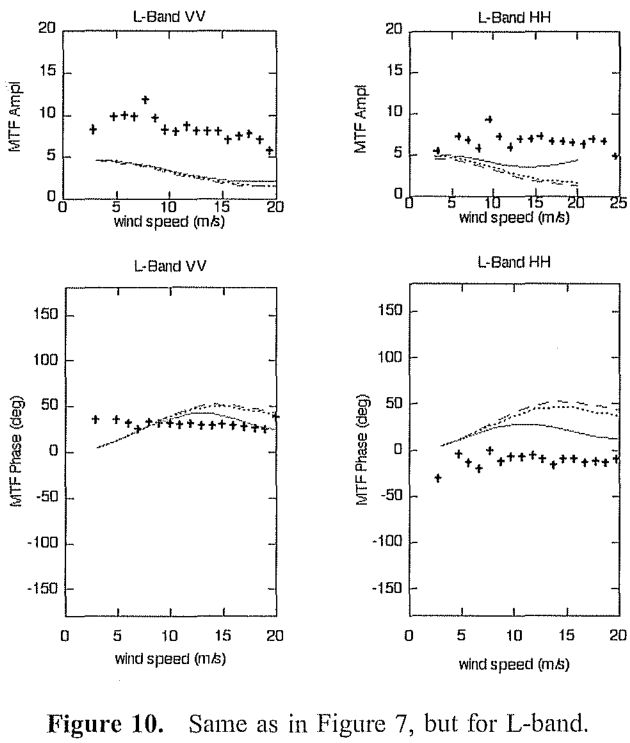

Figure 10. Same as in Figure 7, but for L-band.

scattering model alone, generally fails to reproduce measurements. There is no significant difference between pure Bragg and composite Bragg scattering models. It means that the impact of the modulation of the tilting waves corresponding to the range of intermediate scale is small and may be omitted. In contrast, the impact of wave breaking modulation (supporting non-Bragg scattering) on the hydrodynamic MTF is significant. Due to the latter contribution, the amplitude of the hydrodynamic MTF increases and its phase shifts toward the LW crests. The non-Bragg scattering modulation explains the important experimental finding that the hydrodynamic MTF at HH polarization exceeds that at VV polarization. This feature has been mentioned in the past, but no quantitative explanation was given. The observed larger amplitude of the hydrodynamic MTF for HH polarization can only be attributed to the wave breaking modulations.

[47] To explain the large difference of the hydrodynamic MTF between observations and models based on the Bragg theory, *Hara and Plant* [1994] and *Schmidt et al.* [1995] suggested the presence of a very strong surface stress modulation by LW (with MTF of the order of 10) with its enhancement on the LW crest. However, up to now there is no convincing experimental evidence that such stress variations may exist in reality. In our model, the surface stress modulations are accounted for. They are provided by the airflow undulations over LW and LW-induced variations of the aerodynamic surface roughness. Model calculations presented in Figure 5 show that at low winds, strong wind stress modulations (with the MTF amplitude about 10 or more) can occur, but the fact that the predicted amplification of the stress is over the LW trough is not suggesting this process as a plausible mechanism explaining the observed radar MTF features. On the contrary, at high winds ($U > 10$ m/s) amplification of the surface stress occurs on the LW crest, and its relatively large MTF amplitude (approaching 5) confirms that for such conditions, the suggestions of *Hara and Plant* [1994] and *Schmidt et al.* [1995] can be considered as the most plausible mechanism of SW modulations. However, we again emphasize that only taking into account the wave breaking modulations supporting non-Bragg scattering brings the model to an agreement with observations at both VV and HH polarization.

[48] Most of the experimental estimates of the radar MTF obtained from platform-based radar observations at moderate incidence use the Doppler shift to estimate the LW orbital velocity. LW orbital velocity is then used to estimate the wave height spectra and the radar MTF [e.g., *Plant et al.*, 1983]. In the present paper, such data are taken from the studies of *Hara and Plant* [1994] and *Schmidt et al.* [1995]. *Plant* [1997] however show that the Doppler spectra may not be used with the standard approach to estimate the wave spectrum at incidence angles exceeding 60°. In the present paper, our simulations of radar MTF have not been applied to interpret observations at such high incidence angles. According to our model, wave breaking significantly contributes to the hydrodynamic MTF. Then, the question can arise whether it could also significantly affect the Doppler shift that may result in a wrong estimate of the radar MTF. As it was shown in part 1 the main contribution to the non-Bragg scattering is coming from the shortest breaking waves (see part 1, equation (58)). This is simply due to the fact that the shorter are the gravity waves, the higher is the surface density of their breaking crests. The wavelength of the shortest breaking waves supporting non-Bragg scattering exceeds the radio wave wavelength by a factor of 10. The experimental evidence of the dominating role of the shortest wind waves in white cap coverage and in its modulation by LW was given by *Dulov et al.* [2002]. For Ka, X, and C bands, the scale of breaking waves responsible for NRCS modulation is much less than the LW wavelength (hence they are slow and as well as Bragg waves they are advected by LW orbital motions). Moreover at moderate incidence angles ($40° \leq \theta \leq 60°$) at HH polarization, and at all incidence angles at VV polarization they do not dominate radar returns. Therefore, the impact of wave breaking on experimental radar estimates of the LW steepness via Doppler shift is not significant. An implicit evidence is the well known fact that at moderate incidence (less than 60°) wave height variance spectra can be deduced from Doppler shifts assuming that they are caused by orbital velocities.

[49] In opposite at L-band, the wavelengths of the shortest breaking waves supporting non-Bragg scattering are about 3 m and more. The scale of these waves is not negligible with respect to the LW wavelength, and their phase speed (associated with the speed of wave breaking fronts) may significantly exceed LW orbital velocities. In this case one may anticipate that Doppler shifts along the LW are strongly "contaminated," being in one moment caused by LW orbital motions and in another one being caused by wave breaking. Hence, the radar MTF for L-band may be incorrectly estimated. This may be a reason why observed L-band MTF presented in Figure 10 indicates large MTF amplitudes which by no means can be related to the SW modulations.

6. Conclusion

[50] In part 1, we developed a semiempirical model aimed at the description of the NRCS of the sea surface at HH and VV polarizations, applicable at various radar frequencies, incidence angles, and wind conditions. The model accounts for the Bragg and non-Bragg radio wave scattering components, the latter being associated with breaking waves. Statistical properties of the sea surface (needed for the NRCS computation) are calculated through the wave spectrum, which in turn results from the solution of the energy spectral density balance equation. In the case of steady wind and uniform medium this model describes the background statistical and microwave scattering features of the sea surface.

[51] In part 1, it was shown that the behavior of the sea surface NRCS, and in particular the polarization ratio was correctly reproduced by the model only if the non-Bragg scattering due to breaking waves was taken into account. We further showed here that the contribution of non-Bragg scattering to the total NRCS is larger at HH polarization than at VV polarization, as illustrated in Figure 1.

[52] Because of this important role of wave breaking, it is also necessary to take it into account in the analysis of the radar MTF. This was the purpose of this part 2. When describing the surface, modulation of wave breaking is considered in addition to modulation of Bragg waves. This effect has never been clearly analyzed before. Experimental

ıdy by *Dulov et al.* [2002] showed that wave breaking is ıry strongly modulated by LW, and that wave breaking ıhancement occurs on the LW crests.

[53] The model of wave radar MTF developed here, takes to account the modulation of Bragg and non-Bragg attering characteristics of the sea surface: Bragg waves, ean square slope of the tilting waves (composite Bragg eory), and fraction of the sea surface covered by very ugh surface associated with wave breaking. Variations of ese characteristics along the LW are calculated through the odulation of the wave spectrum. It is found as a solution ' the wave action conservation equation where the source/ ık of wave action keeps the same form as in the back-ound problem (part 1). Effect of the LW on the short wind aves is expressed via their interaction with the LW orbital :locity and with variation of the wind surface stress along e LW. Well inside the capillary range, wave modulations e mainly affected by the mechanism of generation of ırasitic capillaries. Modulation of carrying gravity waves sults in a cascade (and amplified) modulation of capillary aves. Modulation of wind surface stress results from the teraction of the turbulent airflow with the LW possessing e varying aerodynamic roughness. To estimate the varia-ɔn of the stress, it was suggested that the disturbances of rbulent characteristics are concentrated inside a thin IR ljacent to the surface, and the airflow above experiences viscid undulations. Variations of surface roughness along e LW results from modulation of SWs providing the sea rface form drag, which consists of wave-induced momen-m flux to SWs and surface stress supported by the airflow paration from breaking waves. Model estimates showed at large magnitudes of stress modulation (about 10 times e LW steepness) occur at low winds with its intensifica-ɔn over the LW trough. At high winds enhancement of rface stress occurs over the LW crest, but its amplitude is ıaller than at low winds. Our model calculations indicated at suggestions made in a number of other studies [e.g., *ara and Plant*, 1994; *Romeiser et al.*, 1994; *Schmidt et al.*, ɔ95] that strong wind stress modulation is the governing echanism responsible for the large observed amplitude of e hydrodynamic part of the radar MTF with its phase at V crest can be only valid at high wind speeds and for the V polarization.

[54] Our calculations showed that modulations of the ean square slope of tilting waves do not affect consid-ably the hydrodynamic MTF. Thus, the hydrodynamic TF results from modulations of Bragg waves and wave eaking. Since the NRCS for HH polarization is less than r VV, the impact of non-Bragg scattering modulation /hich is independent on polarization) is stronger for the 'drodynamic MTF at HH polarization. This explains that e magnitude of the hydrodynamic MTF at HH polar-ation is larger than that at VV. This fact has been entioned in other studies, but never been explained ıantitatively by wave breaking modulation. In contrast to e pure Bragg hydrodynamic MTF, accounting for the ave breaking may explain the large amplitude of the 'drodynamic MTF, and also the shift of the MTF phase ward the LW crest. Even in conditions where the con-bution of non-Bragg scattering to the total NRCS is not ɔminant (less than 50%), the strong modulations of wave eaking significantly contributes to the radar MTF. At HH polarization, this contribution is of a crucial importance. While pure Bragg models of radar MTF fail to reproduce the observations, our model predictions of radar MTF are consistent with results from observations for both polar-izations and in a wide range of radar frequencies from (Ka-band to C-band) either taken from the literature or obtained for the present study. At L-band, our modeled radar MTF underestimates the observations of *Schmidt et al.* [1995], which indicate amplitudes of the hydrodynamic radar MTF much larger than our model predictions. In this case (L-band), we suggest that the technique used to estimate the radar MTF (based on the Doppler shift of the radar return) may not be appropriate.

[55] In this set of two papers, the main driving parameter is the relative ratio between the Bragg and the non-Bragg scattering mechanism. As developed, this ratio has been consistently derived, according to the wave breaking sta-tistics resulting from the wave energy balance equation. This ratio is enhanced at HH polarization. In contrast to a pure or composite Bragg model, the full model including the non-Bragg mechanism explains the difference between VV and HH for the background NRCS. It also helps to explain larger amplitude modulations near the crest of the long waves.

[56] In the next future, theoretical and experimental investigations should be directed to better assess the occur-rence and distribution of breaking waves associated with enhanced roughness areas, and their radar signature. Such studies will directly serve efforts related to retrieve domi-nant ocean surface waves characteristics from spaceborne Synthetic Aperture Radar. This should also help to better determine breaking wave statistics from remote sensing measurements, and henceforth to quantify from remote sensing the critical role of wave breaking in air–sea transfer.

[57] **Acknowledgments.** We acknowledge the support by EU INTAS-International Association under grants INTAS-CNES-97-02222 and INTAS-CNES-97-1291. V.K. also acknowledges support by the Office of Naval Research under grant ONR N00014-98-1-0653. We acknowledge the support by CNRS for providing a 3-month position to V.K as visiting scientist at CETP in 1999. The FETCH experiment was supported by CNRS/Institut des Sciences de l'Univers (PATOM and PNTS programs), Météo-France, IFREMER, and the program MATER of the European Commission. We are grateful to the one reviewer whose valuable comments stimulated an improvement of the present study.

References

Alpers, W. R., and K. Hasselmann, The two-frequency microwave technique for measuring ocean-wave spectra from an airplane or satellite, *Boundary Layer Meteorol.*, *13*, 215–230, 1978.

Belcher, S. E., and J. C. R. Hunt, Turbulent shear flow over slowly moving waves, *J. Fluid Mech.*, *251*, 109–148, 1993.

Dulov, V., V. Kudryavtsev, and A. Bol'shakov, A field study of white caps coverage and its modulations by energy containing waves, in *Gas Transfer at Water Surface*, *Geophys. Monogr. Ser.*, vol. 127, edited by M. A. Donelan et al., pp. 187–192, AGU, Washington, D. C., 2002.

Grodsky, S. A., V. N. Kudryavtsev, A. N. Bol'shakov, and V. E. Smolov, A field study of wave-induced variations in the radar signal, *Mor. Hydrofizicheski J.*, *4*, 26–40, (in Russian), 1999.

Hara, T., and W. J. Plant, Hydrodynamic modulation of short wind-wave spectra due to long waves measured by microwave radar, *J. Geophys. Res.*, *99*, 9767–9784, 1994.

Hauser, D., and G. Caudal, Combined analysis of the radar cross-section modulation due to the long ocean waves around 14° and 34° incidence: Implication for the hydrodynamic modulation, *J. Geophys. Res.*, *101*, 25,833–25,846, 1996.

Hauser, D., G. Caudal, G. J. Rijckenberg, D. Vidal-Madjar, G. Laurent, and P. Lancelin, RESSAC: A new airborne FM/CW radar ocean wave spectrometer, *IEEE Trans. Geosci. Remote Sens.*, *30*(5), 981–995, 1992.

Janssen, P. A. E. M., H. Wallbrink, C. J. Calkoen, D. Van Halsema, W. A. Oost, and P. Snoeij, VIERS-1 Scatterometer model, *J. Geophys. Res.*, *103*, 7807–7831, 1998.
Keller, W. C., and W. J. Plant, Cross section and modulation transfer function at L and Ku bands measured during the Tower Ocean Wave and Radar Dependence Experiment, *J. Geophys. Res.*, *95*, 16,277–16,289, 1990.
Keller, W. C., and J. W. Wright, Microwave scattering and the straining of wind-generated waves, *Radio Sci.*, *10*, 139–147, 1975.
Kudryavtsev, V., and V. Makin, Coupled dynamics of short waves and the air flow over long surface waves, *J. Geophys. Res.*, *107*, 3209, doi:10.1029/2001JC001251, 2002.
Kudryavtsev, V., C. Mastenbroek, and V. Makin, Modulation of wind ripples by long surface waves via the air flow: A feedback mechanism, *Boundary Layer Meteorol.*, *83*, 99–116, 1997.
Kudryavtsev, V., V. Makin, and B. Chapron, Coupled sea surface atmosphere model, 2, Spectrum of short wind waves, *J. Geophys. Res.*, *104*, 7625–7639, 1999.
Kudryavtsev, V., Malinovskii, A. Bol'shakov, and V. Smolov, A field study of wave-radar modulation transfer function at 37 GHz, (in Russian), *Issled. Zemli Kosmosa*, *4*, 13–30, 2001a.
Kudryavtsev, V., V. Makin, and J. F. Meirink, Simplified model of the air flow above waves, *Boundary Layer Meteorol.*, *100*, 63–90, 2001b.
Plant, W. J., Bragg scattering of electromagnetic waves from the air/sea interface, in surface waves and fluxes, *Remote Sens.*, *II*, 41–108, 1990.
Plant, W. J., A model for microwave Doppler sea return at high incidence angles: Bragg scattering from bound, tilted waves, *J. Geophys. Res.*, *102*, 21,131–21,146, 1997.
Plant, W. J., W. C. Keller, and A. Gross, Parametric dependence of ocean wave-radar modulation transfer function, *J. Geophys. Res.*, *88*, 9747–9756, 1983.
Romeiser, R., A. Schmidt, and W. Alpers, A three-scale composite surface model for the ocean wave-radar modulation transfer function, *J. Geophys. Res.*, *99*, 9785–9801, 1994.
Schmidt, A., V. Wismann, R. Romeiser, and W. Alpers, Simultaneous measurements of the ocean wave-radar modulation transfer function at L, C, and X bands from the research platform Nordsee, *J. Geophys. Res.*, *100*, 8815–8827, 1995.
Schroeder, J., F. Feindt, W. Alpers, and W. C. Keller, Measurements of the ocean wave-radar modulation transfer function at 4.2 GHz, *J. Geophys. Res.*, *91*, 923–932, 1986.

G. Caudal and D. Hauser, Centre d'Etude des Environnements Terrestres et Planétaires, Centre National de la Recherche Scientifique (CNRS), Université de Versailles, Velizy, France. (hauser@cetp.ipsl.fr)
B. Chapron, Institut Francais de Recherche pour l'Exploitation de la Mer, Plouzane, France.
V. Kudryavtsev, Marine Hydrophysical Institute, National Academy of Science, Sebastopol, Ukraine.